Impact-Based Feature Extraction Utilizing Differential Signals of Phase-Sensitive OTDR

Muhammad Adeel, Chao Shang, Diya Hu, Huan Wu, Kun Zhu, Aadil Raza, and Chao Lu

***Abstract*—Traditional vibration pattern recognition of ϕ-OTDR system was operated by event-based feature extractors. The proposed adjacent Spearman correlation assisted algorithm can be considered as impact-based feature extractor utilizing differential signals by extracting the impact region of the perturbation without involving idle data region. This technique can utilize less number of data traces in the pattern recognition process. Classifying with the unique way of impact-based strategy for the direct detected ϕ-OTDR system, both the classification accuracy and processing cost have been improved irrespective of the nature of applied perturbation.**

***Index Terms*—Distributed acoustic sensing, event recognition, perturbation recognition, Phase-OTDR.**

I. Introduction

ALLEVIATING Nuisance Alarm Rate (NAR) was provided much more emphasis on improving the performance of ϕ-OTDR pattern recognition as NAR has a strong connection with the classification accuracy. High accuracy was normally refined at the cost of acquiring a myriad number of traces which eventually boosted the processing delay (T_{pr}) [1]–[6]. Steps were taken by [7]–[9] were aimed at improving classification accuracy and T_{pr} of the system due to the algorithm efficiency. Besides concerning about the recovery of the perturbed signals from the fiber's response from a variety of noise including coherent fading noise effects [10]–[13], differential signals are mainly used for perturbation detection and recognition. There is a possibility that the number of acquired traces influence the dominance of trace-to-trace fluctuation (TTF) based noise. However, the ramifications regarding the effect of acquiring a huge number of data traces were ignored in perturbation recognition applications as previous attempts of algorithm and feature extractor design was not given enough attention in compensating TTF-based noise effects. Another issue with the previous attempts of algorithm design was mostly lacking in avoiding the effect of noise [7], [8], [14] except with time-frequency based algorithms like discrete wavelet transform (DWT) [15]–[18]. In real deployments, the time-frequency based algorithms are intensively parameter-dependent like choosing a very selective mother-wavelet and vanishing moments in DWT-based algorithms to a specific event. It means choosing these parameters to a certain event in a multi-event perturbation recognition application may not be possible as other events are affected by this practice. The severe TTF-based noise is mostly due to the worse line-width and frequency drift of laser source [16], [19], [20] as well as the frequency instability and worse extinction ratio of optical modulator [21], [22]. Hence, the attempts for mitigating TTF-based noise were made by improving the performance of these optical components which were meant to deploy the systems with complex structures and higher costs.

Instead of targeting components up-gradation or parameter-intensive algorithm design, the alleviation of TTF-based noise was by-passed with the help of best classifier-based approach a high emphasize of which started after the year 2015 [3], [23]–[27] followed by the deep neural network approach [5], [6]. However, improving the classifier-based approach leads to the concept of non-robust feature extraction stage as the [28] reveals that an increase in the learning machine generalization is the motivation of the best feature extractor. Moreover, an implementation of very high processing classifiers like the deep neural network does not suit well to ϕ-OTDR based applications due to the involvement of comparatively very fewer amount of data in these applications. More data means more data traces and a very large delay due to the round trip of all the acquired data traces. TTF-based noise effect has an adverse effect on classification accuracy in perturbation recognition applications as it leads to a variation in patterns of the few useful differential signals against a certain perturbation.

The pattern recognition among different perturbations in ϕ-OTDR system was restricted to event-based feature extraction [1], [2], [7], [25], [27]. This event-based feature extraction

Manuscript received September 4, 2019; revised November 13, 2019 and December 9, 2019; accepted December 28, 2019. Date of publication January 13, 2020; date of current version April 15, 2020. This work was supported in part by the National Natural Science Foundation of China (NSFC) under Grant U1701661 and in part by The Hong Kong Polytechnic University under Grant 1-YW0S, Grant 1-YW3G, Grant 1-ZVFL, and Grant H-ZG7E. *(Corresponding author: Chao Shang.)*

M. Adeel, D. Hu, H. Wu, K. Zhu, and C. Lu are with the Photonics Research Centre, Department of Electronic and Information Engineering, The Hong Kong Polytechnic University, Hung Hom, Kowloon, Hong Kong, China, and also with the Hong Kong Polytechnic University Shenzhen Research Institute, Shenzhen 518057, China (e-mail: m.adeel@connect.polyu.hk; 15103937d@connect.polyu.hk; nuaawuhuan@gmail.com; kun.zhu@polyu.edu.hk; enluchao@polyu.edu.hk).

C. Shang is with the Key Laboratory of Luminescence and Optical Information, Ministry of Education, Institute of Optical Information, School of Science, Beijing Jiaotong University, Beijing 100044, China, with the Photonics Research Centre, Department of Electrical Engineering, The Hong Kong Polytechnic University, Hung Hom, Kowloon, Hong Kong, China, and also with the Hong Kong Polytechnic University Shenzhen Research Institute, Shenzhen 518057, China (e-mail: cshang@bjtu.edu.cn).

A. Raza is with Physics Department, COMSATS Institute of Information Technology, Islamabad 45550, Pakistan (e-mail: aadilraza@comsats.edu.pk).

Color versions of one or more of the figures in this article are available online at https://ieeexplore.ieee.org.

Digital Object Identifier 10.1109/JLT.2020.2966413

strategy was less efficient for classifying non-continuous activities. Nevertheless, the perturbation events can be separated into more elaborate parts. For example, a man running on the ground is the non-continuous activity which involves the impact of feet upon the ground and the idle data between these impact-based active regions, and a combination of both types data makes up a single event. Therefore, in this paper we have proposed an impact-based feature extraction solution for perturbation recognition only, focusing on the active region of the perturbed trace, where the data along the slow-axis correspond to the external impact of the applied force. These benefits include an improvement in classification accuracy and the algorithms capability to perform impact-based feature extraction to best suit the multi-event recognition application.

Features based on adjacent Spearman correlation of data-vectors was proposed which acts like a non-parametric Matched Filtering (MF) to extract the exact boundaries of the vibration location [29] in addition to the removal of TTF-based noise effects, leaving behind the effect due to necessary phase change only. Impact-based features can be extracted with the help of the same MF-based algorithm by attributing the exact boundaries of active region along the slow axis of the perturbed region, which in turn provides a possibility of using parameter estimation in conjunction with impact-based recognition to further boost the classification accuracy without providing the idle data directly to the classifier. With this technique, impact-based feature extraction reduces the data usage and has a more efficient processing strategy in addition to simultaneously maintaining a high pattern recognition accuracy. As the coherent detected systems are well known in DAS systems, the use of simple structure direct detected system in the recent articles can never be neglected because of its low cost and a wide installation [3], [15], [24], [25], [27], [30]–[33]. Due to this reason, the emphasis of algorithm improvement was given to improve the performance of direct detected ϕ-OTDR system in this paper.

II. Theoretical Model

Assuming one integrated backscattering center under each sampling length of δL, the optical power for the same segment against each trace can be expressed as in Eq. (1).

$$I(u) = 2E_0^2 exp(-2a_f u \Delta L) r_u^2 \sum_{q}^{N_{p/2}} \sum_{s=q+1}^{N_{p/2}-1} \ldots \left[\cos(\phi_q - \phi_s) + N_{p/2}\right] \quad (1)$$

where a_f is the loss coefficient of fiber, r_u is the back-scattering rate of each sampling length, $(\phi_q - \phi_s)$ is the phase difference among the integrated backscattering centers, and $N_{p/2}$ is the number of integrated backscattering center in half-width of injected pulse behind the sampling location along the forward direction of the fiber under test (FUT).

The differential trace is represented as $\delta_i(n) = I_i(n) - I_{i+1}(n)$, where $\{i \in \mathbb{N}, n \in \mathbb{N} : 1 \leq n \leq N_r\}$, and N_r is the total number of samples along fast-axis within a single processing window. A sketch representing different parameters of the received RBS signal is demonstrated in Fig. 1. A processing window marked by a red frame is dragged along slow-axis in the perturbed region with a step of length α. One processing window can be divided into N_r data vectors and each of these data-vectors is comprised of β number of data points in slow-axis, represented by a green line. The TTF-based noise ϕ_n affects each differential signal and this phase impersonates the additional phase θ_p due to the applied perturbation. A combined effect of both of these phases is represented by $\varphi_p \approx \mathcal{F}(\varphi_n + \theta_p)$. It means the resultant phase φ_p cannot be a direct function of the originally perturbation-induced phase θ_p due to the involvement of non-necessary effects with its phase φ_n. The need here is to apply the correlation on adjacent data-vectors on top of differential signals that must be used to alleviate the effect of φ_n such that $\varphi_p \approx \mathcal{G}(\theta_p)$. MF-based technique based on Spearman correlation coefficient can be used to eliminate the effect of φ_n. This coefficient is termed $R[n]$ and it is applied to the rank defined by each adjacent data-vectors n, termed δ_j, which for a single drag of a processing window can be computed as,

$$R[n] = 1 - \frac{6\sum_{i=1}^{\beta}(r_g[\delta_i(n)] - r_g[\delta_i(n+1)])^2}{\beta(\beta^2 - 1)} \quad (2)$$

where r_g is the rank of each data-vector. If there are total K number of jumps of this window, $R_k[n]$ represents Spearman correlation coefficient of the nth and $(n+1)th$ data vectors against each kth movement as $k = 1, 2, \ldots K$.

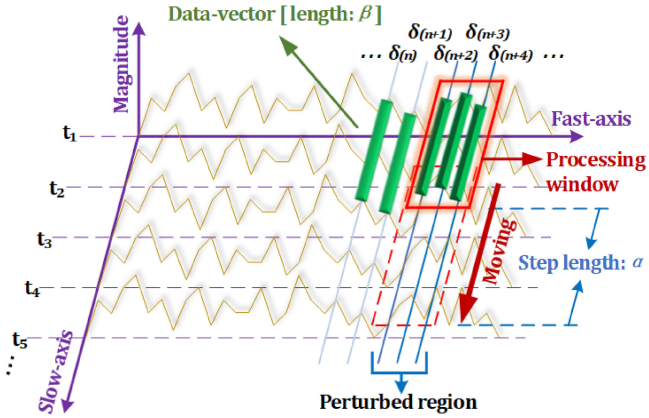

Fig. 1. A demonstration of the basic terminologies.

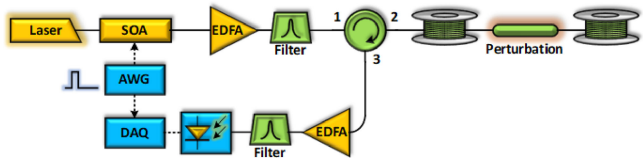

Fig. 2. Basic demonstration of the experimental setup.

III. Experimental Work and Analysis

The experiment was conducted using a direct detected OTDR system as shown in Fig. 2. The injected pulse is modulated by a semiconductor optical amplifier (INPHENIX: IPSAD1501) with the help of a narrow linewidth laser source (NKT: X15 Linewidth $<$ 0.1KHz) of 1550.12 nm. The two Erbium-Doped

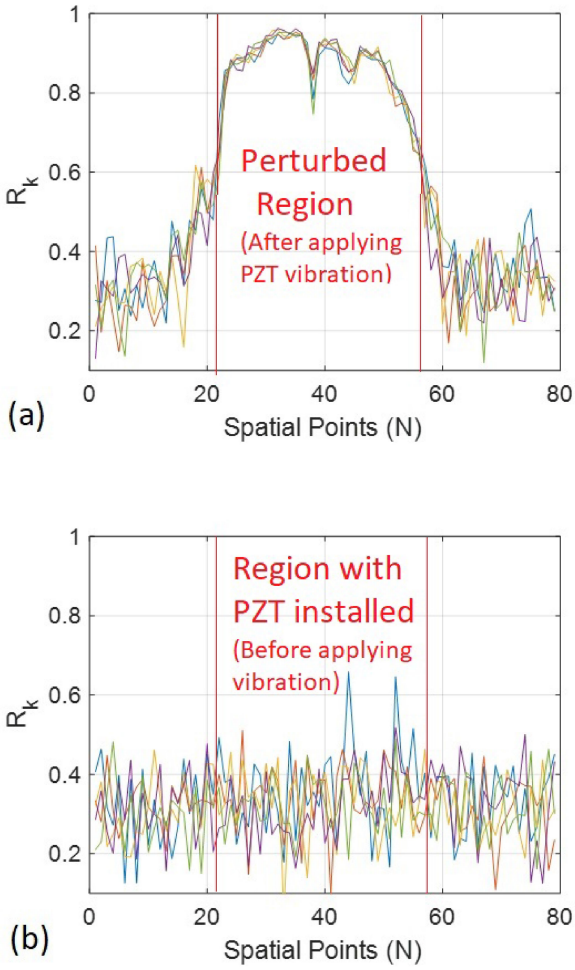

Fig. 3. Each color represents the result of R_k against each kth data-set, (a) with Perturbation and (b) without Perturbation.

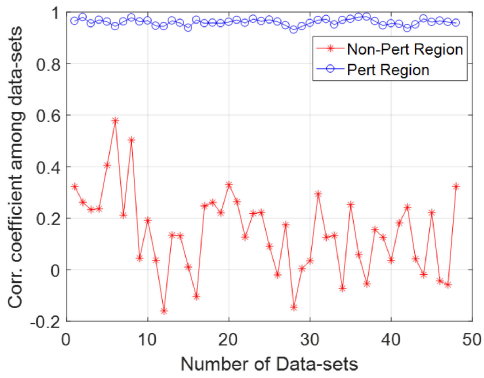

Fig. 4. Correlation coefficient for 48 different data-sets including both perturbed and non-perturbed regions.

Fiber Amplifiers (Amonics: AEDFA-PA-35) are employed for amplifying the pulse and the backscattering signal, and the amplified spontaneous emission noise was removed by the filters with 3 dB bandwidth of 0.6 nm. Using a data acquisition card of 250 MHz sampling rate (SPECTRUM: M4i), there is an equal gap of 0.4 m among all the data-vectors. Different PZT based, real motor-based vibration and real non-continuous activity-based perturbations were provided. All the experiments were carried out with a 7.5 km FUT followed by the perturbation sources which is further followed by an 800 m fiber before a termination point. The fiber length under the effect of perturbation has been considered 1 m in case of real noncontinuous activity and motor-based vibration whereas it was 10 m in case of PZT-based vibration. The time resolution of the perturbation response signal was based on the pulse-repetition rate at 10KHz (0.1 ms) in all experiments.

The perturbation-induced phases represent a primary phase change. Due to other non-necessary effects, the primary phase change by the fiber elongation is disturbed. In the proposed method, the primary phases among RBS signals are matched after applying the correlation operator. Fig. 3 shows the results before and after applying the 100 Hz square wave perturbation using the window width of 80 spatial points that moves with a step-length of $\alpha = 200$ and a data-vector length of $\beta = 200$ after considering 5 data-sets from the whole data. Part (a) of the same figure represents the effect of perturbation as a result of applying MF-based algorithm, as in Eq. (2), after using different data-sets at a specific location of perturbations. Each kth data-set in the figure is represented by a specific color in this figure with the same conditions like position and the nature of perturbation except different time-instants. A strong similarity can be seen among the results of different data-sets as the effect of primary phase change is similar across all data-vectors within the perturbed region. The perturbed region can be distinguished from the non-perturbed region by the two obvious boundaries in the Fig. 3(a) and each kth data-set is shown to provide almost a similar response. Fig. 3(b) shows the results of applying the proposed MF-based feature extractor without applying any perturbation. These results do not show any relation between different data-sets nor does they show an increase in correlation among different data-vectors in a single data-set. This clearly shows the effect due to different noise effects without the involvement of the effect of primary phase change. Considering the range of correlation coefficient among different data-sets between -1 (inverse relation) and +1 (similar relation), the mentioned correlation coefficient of the non-perturbed and perturbed parts were calculated which can be seen in Fig. 4. This index was measured against 48 different data-sets, each data-set is mutually independent and was composed of $\beta = 200$.

The common feature extractors in the field of ϕ-OTDR pattern recognition are time-series or a frequency spectrum based, which according to the latest review [34], have been used 84% of the time of all the feature extractors used. The reason is that the feature extraction stage can be any of the three categories including time-series or the original differential data, frequency-based or time-frequency based where due to an intensive parameter adjustment for each type of event, the time-frequency based feature extraction is normally ignored in perturbation recognition applications. For these reasons, we have used Level Crossing (LC) and Short-Time-Fourier Transform (STFT) as the example for both time and frequency based feature extraction. The results from these feature extraction were compared with the proposed feature extraction.

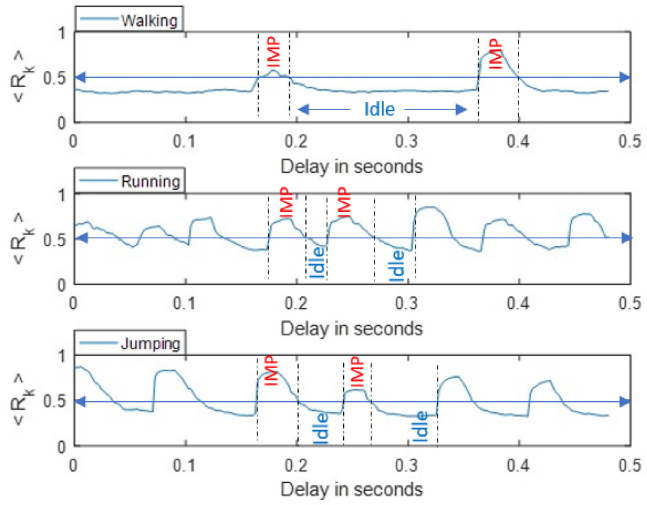

Fig. 5. Intensity variation representation of three activities (walking, running, and jumping) using MF algorithm.

In Eq. (3), $L[p]$ represents the number of times the pth level is attained by the given differential signal and N_l is the total number of levels attributed between the boundaries of the extreme amplitudes of the given differential signal.

$$L\left[p\right] = \sum_{t=0}^{\beta-2} \mathcal{J}\left[\delta(t) < \varepsilon(p) \;\; \& \;\; \delta(t+1) \geq \varepsilon(p)\right] \qquad (3)$$

where the function $\mathcal{J}(y)$ is either 1 or 0 for true and false conditions respectively and p counts from 0 to $N_l - 1$. The term $\varepsilon(p)$ represent each pth threshold.

The NFFT points in-case of STFT is assumed to have N_f points against each computing window. The relation can be computed as,

$$F\left[\omega\right] = \sum_{t=0}^{\beta-1} \delta(t) e^{-j\omega t} \qquad (4)$$

where ω ranges from 0 to $N_f - 1$.

The output of feature extractors $(L[p], F[\omega], R[n])$ was provided to the Random Forest (RF) classifier with 5 trees and the error of detecting False Alarms by using the proposed extractor was compared with the results of traditionally used feature extractors. A ratio of 10/90 of training/validation has been used throughout the experiments where RF classifier was used. The purpose of attributing a very small proportion of training data with RF classifier is that it belongs to the class of bagging classifiers and provides importance to the inherent characteristics of the input data despite the training data to better differentiate among events. To keep a similar T_{pr} in case of all the three feature extractors, 10-fold cross-validation with $\beta = 20$ and $\alpha = 1$ was used when considering non-continuous activities analogous to walking, running and jumping. If $< R_k >$ represents the average of each kth processing window, the behavior of these activities can be seen in Fig. 5. By assuming a threshold of 0.5 for segregating idle data from that of impact based data, we consider the impact part of the data that exceeds the threshold. Before feeding the feature extracted data to any classifier, we can assess the performance of MF-based algorithm in comparison to the original signal and the differential signal processing with STFT and LC algorithm.

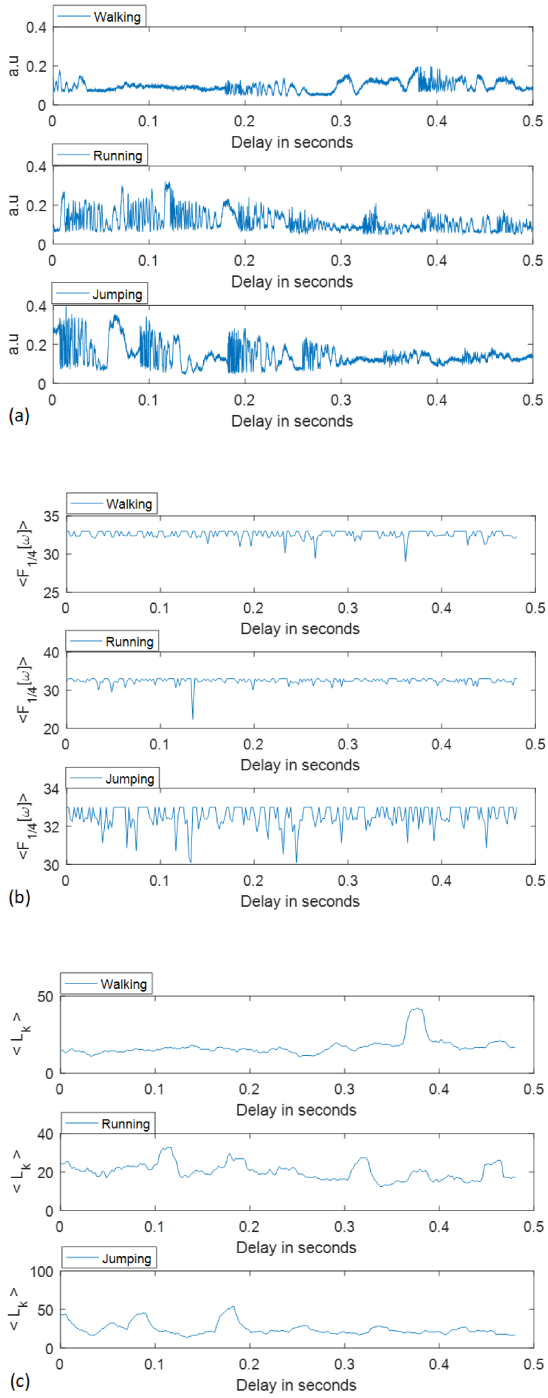

Fig. 6. Intensity variation representation of three activities (walking, running, and jumping) using (a) original data, (b) STFT-transformed data, and (c) LC-transformed data.

Before jumping to the application of any machine learning algorithm to classify different events, the non-continuous type of perturbation can be seen in the perspective of original data as it can be seen in Fig. 6(a). This plot was obtained as a result of

plotting the original data (before any further processing) in time-domain within the perturbed region of the three non-continuous activities. Due to the worst visualization, the results from STFT transformation in Fig. 6(b) are obtained by plotting the frequency of dominant region in the processing window against the spatial resolution. The FFT index at which the amplitude of the STFT is more than 1/4 of the average of FFT of the whole data, termed $F_{1/4}[\omega]$, is considered in this case but the results are not promising with the optimum conditions of the data. The term 1/4 was considered as the level of the average of the FFT of the whole data was almost equal to 1/4 of the highest FFT value of the processing window with $\beta = 200$. If the same number of data traces are considered in case of LC feature extractor, the average of each kth processing window using LC feature extractor can be represented by $< L_k >$. For exactly the same activity and keeping in view all the conditions as these were given in Fig. 5, the results using LC feature extractor can be seen in Fig. 6(c). This figure clearly indicates the performance by not visualizing the low intensity perturbation which is due to the existence of a huge number of TTF-based data traces within the perturbed region.

MF-based algorithm does not only help in mitigating TTF-based noise effects but it can also be used in decreasing the requirement of acquiring the number of data-traces. For-instance, considering 20,000 traces [1]–[3], [24], [35] against a 100 km FUT means a delay of 20 sec in acquiring the requisite number of data traces in addition to the delay T_{pr}. If the MF-based algorithm is used as feature extractor, it not only mitigates T_{pr} but also decreases a requirement of acquiring non-essential data traces. Hence, MF-based algorithm can be said to decrease the delay in two different scenarios. In first scenario of non-continuous type of perturbations only, the delay is decreased by lowering T_{pr} due to processing the impact-based data only and ignoring the idle data. In the second scenario where in case of either continuous or non-continuous type of perturbation, the MF-based algorithm is helpful in decreasing the delay at two steps. First by lowering the acquisition of a number of data-traces which declines the round-trip delay and second with a decrease in T_{pr} due to processing less number of data-traces. To verify different scenarios of delay, we will first prove the processing in case of all the three algorithms (LC, STFT and MF) which takes almost similar processing time if the same number of data traces in each case is considered, irrespective of considering a boost in classification accuracy by the MF-algorithm. This can be verified here with the help of processing both the continuous and non-continuous type of perturbation as in Table I. It means all the three algorithms take almost the same processing time. These calculations were made in reference to non-continuous (walking, running and jumping) as well as the continuous-based activities (motor-based, PZT-based). Details of the motor-based vibrations will be provided later in this section. The PZT-based vibration was provided by using a 10 m fiber wrapped around the fiber and a 10-Hz sinusoidal signal was provided to simulate the continuous activity. The values of $\alpha = 1$ and $\beta = 200$ were considered in all these cases. The results in Table I are displayed in seconds after a tic/toc command was used in Matlab and are based on a Gen-7 computer with core-i7 processor with 3.1 GHz speed and 4 M cache. A confusion matrix is one that provides the information about false nagatives and positives and with multiple event case, the confusion matrix provides the error about the detection of false occurrence of a certain event at the a_{ij} element of the matrix for $i \neq j$. Hence, the total error against a certain event is the addition of a_{ij} elements for $i \neq j$, and for all the three events, a certain 3D coordinate is spotted on the 3D plot in Fig. 7. In our case, a 3×3 confusion matrix is formed as a result of three non-continuous activities (Walking, Running and Jumping). Each confusion matrix is formed after validating the mentioned three activities against a training model. This training model was established from RF-based classifier using all the three activities. Fig. 7 shows different results based on the three axes that take in the cumulative error from a confusion matrix. Each of these matrices are derived using the 100 observations in Fig. 7(a) and 200 observations in (Fig. 7(b),(d)). Parts (a,b,c) of the Fig. 7 are based on the non-continuous type of perturbations and each axis of this figure in non-continuous type of activities represents the total error of confusion matrix with respect to running activity (x-axis), walking activity (y-axis) and jumping activity (z-axis). Fig. 7(c) compares the data of MF with that of MF_IM (MF algorithm applied to impact-based region) extractor from both part (a) and part (b) of the same figure, whereas, Fig. 7(d) represents the same confusion matrix based error using the data acquired with the motor-based vibration on a wooden bench in which each axis represents the error against different intensities. We can see the MF-based (MF and MF_IM) feature extractor is better than both LC and STFT based extractors. Moreover, the MF_IM based data exhibits less error as compared to the same technique with both impact and idle based data in addition to saving processing cost which verifies a reduction in a first scenario of delay by the MF-based algorithm. For-example, if the duration of impact is only 20% of the whole duration which means the idle data is accounted for 80% of this duration. In addition to decreasing the error, the processing cost can be reduced 5 times as only the useful data need to be processed in the impact-based processing with the help of MF-based algorithm.

TABLE I
COMPARISON OF T_{pr} (IN SECONDS) BY LC, STFT, AND MF-BASED ALGORITHMS USING THREE DIFFERENT ITERATIONS

	Iter	Walk	Run	Jump	Motor	PZT
STFT	1	33.89	34.85	36.74	34.54	34.75
	2	34.75	35.65	34.21	37.24	33.98
	3	33.93	33.63	36.01	35.16	34.19
LC	1	34.28	38.45	34.43	37.23	38.29
	2	34.21	34.10	34.53	37.08	35.66
	3	39.95	41.04	34.79	35.31	36.39
MF	1	36.73	34.91	34.59	35.42	34.99
	2	34.88	34.35	35.43	35.17	34.54
	3	34.63	36.75	36.60	35.30	34.74

Before going into the details of pattern recognition we consider examples of the patterns made within the impact region. To see the patterns of the impact-based region only we take an example of vibrations using a motor creating vibrations on a wooden board as shown in Fig. 8(a). The motor-based vibration with three different intensities was observed. Fig. 8(b) demonstrates the highly diversified nature as a result of three different activities using MF_IM based feature extractor at different

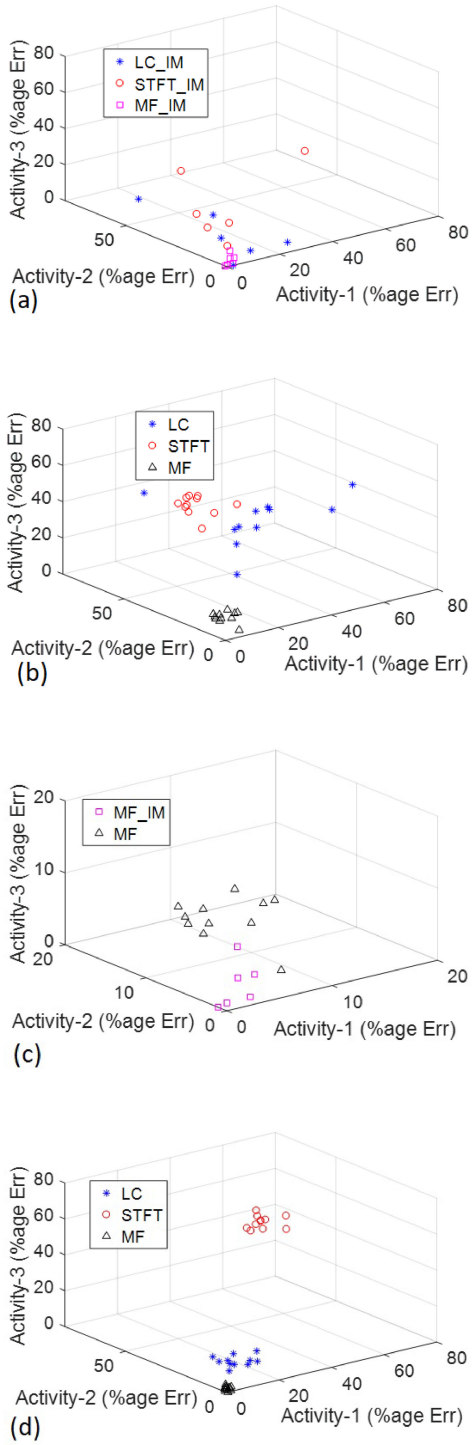

Fig. 7. Using $\beta = 20$ and CV $= 10$ using (a) impact-based data, (b) whole data including impact and idle parts of the data, (c) comparison of MF and MF_IM using both part-a and b, and (d) whole data of continuous activity.

instants, showing the proposed MF_IM-based feature extraction to provide a time-invariant response. Using the same vibration parameters, eight different data-sets at different timings are collected and almost similar performance has been observed throughout against a certain applied perturbation. These patterns are different for different applied perturbations within the impact region. A different color graph in each subplot represents a different data-set.

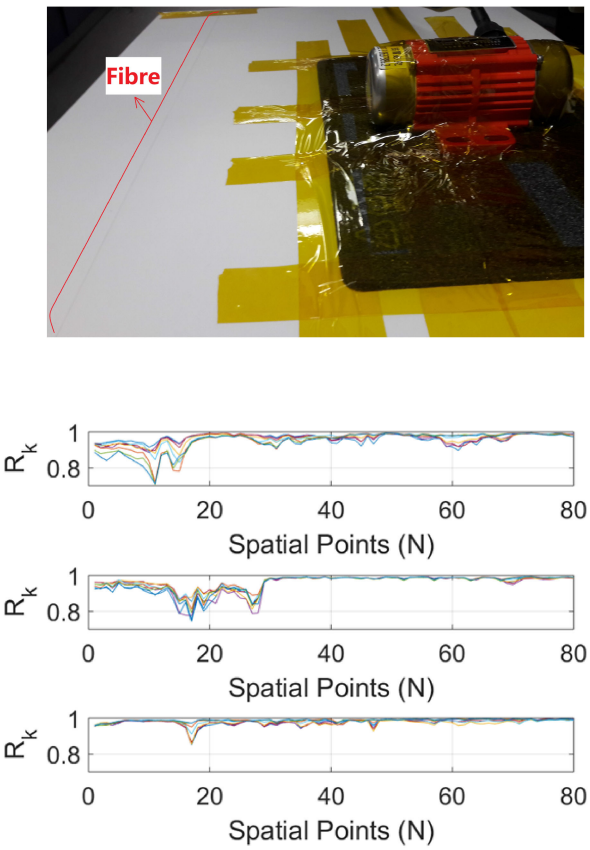

Fig. 8. (a) Demonstrating the motor-based setup (b) results of the MF_IM-based feature extractor after perturbing the fiber with, (Upper) Low Intensity Vibration; (Mid) Moderate Intensity Vibration; (Lower) High Intensity Vibration.

To simplify the analysis, we will deal with the continuous data in the rest of this paper and the reason is that the whole data in that of continuous type of activity represents the impact based data only. It is sometimes difficult to decide a suitable feature extractor if the exact nature of events is unknown. For example, activities differentiated with respect to frequency, amplitude or a combination of both these attributes represent the nature of activities upon which these are differentiated. Fig. 9 demonstrates the performance with respect to the classification metric and two parts of the same figure demonstrate the results with the use of different spatial resolution and with exactly different nature of perturbations. 200 observations were used against each activity that accounts for a total of 800 observations for a total of 4 activities. The system is first learned using 10% of the training data and 90% of the data was used for validation. The results show that the system with our proposed feature extractor performs well than LC if a combination of amplitude and frequency-based variations are introduced in applied perturbation to the FUT by considering the same length of each resultant output vector. In Fig. 9 we can see that the out-performance by the proposed feature extractor is independent of the type of events used. Both Fig. 7 and Fig. 9 exhibits poor performance of STFT without using hyperparameter optimization for a given number of FFT points. These results show that for achieving almost similar performance in classification accuracy in impact based perturbations, the systems with the use of proposed feature extractor

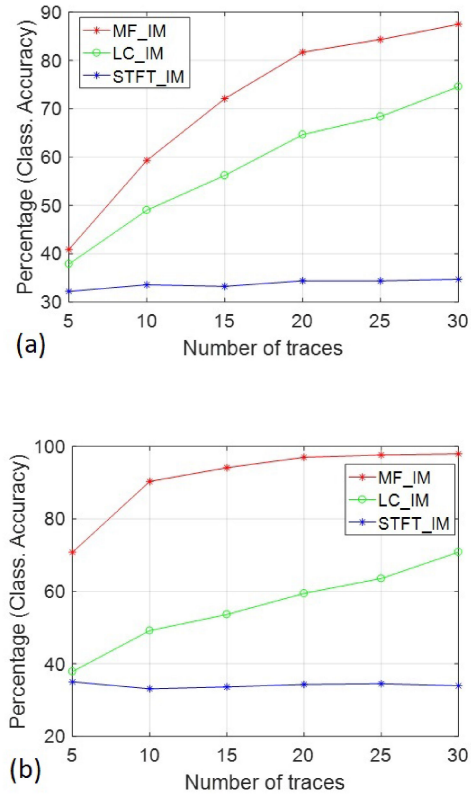

Fig. 9. Classification accuracy in percentage with CV = 10, (a): If amplitude modulated signals are used, where activities are differentiated w.r.t f(AM)[30 Hz], Dept[50%]; f(AM)[30 Hz], Dept[60%]; f(AM)[40 Hz], Dept[50%]; f(AM)[40 Hz], Dept[60%],); 480 ns PW (b): if Motor vibrations are used; 640 ns PW.

reduces a need to a large number of traces as compared to that of other feature extractors. This reduction in a requirement of data-traces not only reduces the delay due to acquiring non-necessary data traces for processing a certain event but also reduces T_{pr} further which verifies the second scenario of avoiding delay due to the MF-based algorithm. For-example, with the use of motor-based vibration data, the MF-based algorithm acquires 5 times less data as compared to the LC-based algorithm for achieving the same classification accuracy as shown in Fig. 9(b). It means a 5 times less data is required if the LC-based algorithm is replaced with the MF-based algorithm using the motor-based vibration. Hence, if the round-trip time taken by all the acquired data-traces by a certain DAS system is 20 sec, it can be to 5 sec in the given example. Furthermore, this huge reduction in the requirement of data-traces reduces the T_{pr} further as the system has to process 5 times less data if MF-based algorithm is used instead of LC-based algorithm in the given example.

Proving the out-performance of our proposed solution with the use of a single classifier might be biasing. To demonstrate the results independent of any classifier and without considering the limits of processing cost, we have used four different classifiers with the optimized hyper-parameters as shown in Table II. Three PZT-based experiments conducted with Exp-1 and Exp-3 were meant to provide four different AM (Amplitude Modulated) signals respectively to the PZT, whereas, Exp-2 was conducted

TABLE II
CLASSIFICATION ACCURACY (IN PERCENTAGE) OF THE TWO BASIC FEATURE EXTRACTORS COMPARED WITH THAT OF PROPOSED EXTRACTOR USING DIFFERENT CLASSIFIERS WITH $\beta = 10$

	FE	C5.0	GBM	Tree Bag	RF
Exp-1	MF_IM	88.52	88.69	86.98	91.65
	STFT_IM	59.07	46.73	55.82	62.66
	LC_IM	36.08	39.08	39.67	39.75
Exp-2	MF_IM	99.83	100	98.37	100
	STFT_IM	95.16	94.74	92.82	96.15
	LC_IM	71.96	74.13	72.17	72.71
Exp-3	MF_IM	91.32	92.82	91.53	95.45
	STFT_IM	55.90	50.19	54.98	58.45
	LC_IM	33.20	38.71	38.03	38.21

by providing four different sinusoids to the same PZT with the perturbation exposed with a 10 m length. Based on the continuous type of perturbations, the percentage accuracy of classification performance by our proposed feature extractor was compared against both types of feature extractors if used directly with differential signals. This increase was observed with respect to both boosting (C5.0 and GBM) and bagging based classifiers (Tree-bag and RF). A very large improvement was observed in the STFT part of Exp-2 in Table II as the STFT performs much better if hyper-parameters of a specific feature extractor are optimized, though the same was not justified with the results of Fig. 7 and Fig. 9 due to the non-favor situation of the events if STFT is used as a feature extractor. Yet, in any case, we cannot see any degradation in the performance of the proposed extractor in comparison to other two feature extractors, which shows the fact that improvement in case of the proposed extractor is always better.

IV. CONCLUSION

For a certain number of acquired traces, our proposed algorithm designed for impact-based feature extractor was proved to perform better by improving the classification accuracy of direct detected system. These improvements were achieved by conducting both feature extraction and noise removal in a single step process without any parameter adjustment as we can see in time-frequency based feature extraction. These characteristics enabled the MF_IM-based feature extraction to best suit in any perturbation recognition application independent of the nature of the events involved. In case of a non-continuous type of perturbations, this technique is much beneficial as in addition to the removal of noise effect, there is a possibility of avoiding idle traces due to its impact based feature extraction capability which in return decreases T_{pr} further which verifies the first scenario of delay saving and it is valid for non-continuous type of perturbations only. Using any type of perturbation (continuous or non-continuous), a reduction in delay by the proposed solution is possible in two ways which verifies the second scenario of saving the delay. These include the time saving in case of acquiring a very less number of data traces to achieve the similar classification accuracy and secondly, T_{pr} is reduced further due to processing of a less number of data traces.

REFERENCES

[1] J. Tejedor *et al.*, "Toward prevention of pipeline integrity threats using a smart fiber-optic surveillance system," *J. Lightw. Technol.*, vol. 34, no. 19, pp. 4445–4453, Oct. 2016.

[2] J. Tejedor *et al.*, "A novel fiber optic based surveillance system for prevention of pipeline integrity threats," *Sensors*, vol. 17, no. 2, 2017.

[3] J. Tejedor, J. Macias-Guarasa, H. Martins, S. Martin-Lopez, and M. Gonzalez-Herraez, "A contextual GMM-HMM smart fiber optic surveillance system for pipeline integrity threat detection," *J. Lightw. Technol.*, vol. 37, no. 18, pp. 4514–4522, 15 Sep. 2019.

[4] X. He *et al.*, "Multi-event waveform-retrieved distributed optical fiber acoustic sensor using dual-pulse heterodyne phase-sensitive OTDR," *Opt. Lett.*, vol. 42, no. 3, pp. 442–445, Feb. 2017.

[5] Y. Shi, Y. Wang, L. Zhao, and Z. Fan, "An event recognition method for Φ-otdr sensing system based on deep learning," *Sensors*, vol. 19, no. 15, p. 3421, 2019.

[6] Z. Wang *et al.*, "Practical multi-class event classification approach for distributed vibration sensing using deep dual path network," *Opt. Express*, vol. 27, no. 17, pp. 23 682–23 692, Aug. 2019.

[7] Q. Sun, H. Feng, X. Yan, and Z. Zeng, "Recognition of a phase-sensitivity OTDR sensing system based on morphologic feature extraction," *Sensors*, vol. 15, no. 7, pp. 15 179–15 197, 2015.

[8] X. Hui, S. Zheng, J. Zhou, H. Chi, X. Jin, and X. Zhang, "Hilberthuang transform time-frequency analysis inϕ-otdr distributed sensor," *IEEE Photon. Technol. Lett.*, vol. 26, no. 23, pp. 2403–2406, Dec. 2014.

[9] W. Zhaoyong, P. Zhengqing, Y. Qing, C. Haiwen, Q. Ronghui, and F. Zujie, "Fast pattern recognition based on frequency spectrum analysis used for intrusion alarming in optical fiber fence," *Chinese J. Lasers*, vol. 42, no. 4, 2015, Art. no. 0405010.

[10] X. Wang *et al.*, "Interference-fading-free Φ-otdr based on differential phase shift pulsing technology," *IEEE Photon. Technol. Lett.*, vol. 31, no. 1, pp. 39–42, Jan. 2019.

[11] Z. Qin, T. Zhu, L. Chen, and X. Bao, "High sensitivity distributed vibration sensor based on polarization-maintaining configurations of phase-OTDR," *IEEE Photon. Technol. Lett.*, vol. 23, no. 15, pp. 1091–1093, Aug. 2011.

[12] P. Healey, "Fading in heterodyne OTDR," *Electron. Lett.*, vol. 20, no. 1, pp. 30–32, Jan. 1984.

[13] H. Liu *et al.*, "True phase measurement of distributed vibration sensors based on heterodyne φ-OTDR," *IEEE Photon. J.*, vol. 10, no. 1, pp. 1–9, Feb. 2018.

[14] P. Stajanca, S. Chruscicki, T. Homann, S. Seifert, D. Schmidt, and A. Habib, "Detection of leak-induced pipeline vibrations using fiberoptic distributed acoustic sensing," *Sensors*, vol. 18, no. 9, 2018, Art. no 2841.

[15] H. Wu, S. Xiao, X. Li, Z. Wang, J. Xu, and Y. Rao, "Separation and determination of the disturbing signals in phase-sensitive optical time domain reflectometry (ϕ-OTDR)," *J. Lightw. Technol.*, vol. 33, no. 15, pp. 3156–3162, Aug. 2015.

[16] Z. Qin, L. Chen, and X. Bao, "Wavelet denoising method for improving detection performance of distributed vibration sensor," *IEEE Photon. Technol. Lett.*, vol. 24, no. 7, pp. 542–544, Apr. 2012.

[17] Q. Li, C. Zhang, and C. Li, "Fiber-optic distributed sensor based on phase-sensitive OTDR and wavelet packet transform for multiple disturbances location," *Optik*, vol. 125, no. 24, pp. 7235–7238, 2014.

[18] Y. Shi, H. Feng, and Z. Zeng, "A long distance phase-sensitive optical time domain reflectometer with simple structure and high locating accuracy," *Sensors*, vol. 15, no. 9, pp. 21 957–21 970, 2015.

[19] Y. Koyamada, M. Imahama, K. Kubota, and K. Hogari, "Fiber-optic distributed strain and temperature sensing with very high measurand resolution over long range using coherent OTDR," *J. Lightw. Technol.*, vol. 27, no. 9, pp. 1142–1146, May 2009.

[20] X. Zhong *et al.*, "Influences of laser source on phase-sensitivity optical time-domain reflectometer-based distributed intrusion sensor," *Appl. Opt.*, vol. 53, no. 21, pp. 4645–4650, Jul. 2014.

[21] H. F. Martins, S. Martin-Lopez, P. Corredera, P. Salgado, O. Frazão, and M. González-Herráez, "Modulation instability-induced fading in phase-sensitive optical time-domain reflectometry," *Opt. Lett.*, vol. 38, no. 6, pp. 872–874, Mar. 2013.

[22] H. F. Martins, S. Martin-Lopez, P. Corredera, M. L. Filograno, O. Frazão, and M. Gonzlez-Herrez, "Coherent noise reduction in high visibility phase-sensitive optical time domain reflectometer for distributed sensing of ultrasonic waves," *J. Lightw. Technol.*, vol. 31, no. 23, pp. 3631–3637, Dec. 2013.

[23] H. F. Martins *et al.*, "Early detection of pipeline integrity threats using a smart fiber optic surveillance system: The pit-stop project," in *Proc. 24th Int. Conf. Opt. Fibre Sensors.*, 2015, Paper 96347X.

[24] J. Tejedor, J. Macias-Guarasa, H. F. Martins, S. Martin-Lopez, and M. Gonzalez-Herraez, "A Gaussian mixture model-hidden Markov model (GMM-HMM)-based fiber optic surveillance system for pipeline integrity threat detection," in *Proc. 26th Int. Conf. Opt. Fiber Sensors*, 2018, Paper WF36.

[25] H. Jia, S. Liang, S. Lou, and X. Sheng, "A k -nearest neighbor algorithm-based near category support vector machine method for event identification of φ -OTDR," *IEEE Sensors J.*, vol. 19, no. 10, pp. 3683–3689, May 2019.

[26] L. Liu, W. Sun, Y. Zhou, Y. Li, J. Zheng, and B. Ren, "Security event classification method for fiber-optic perimeter security system based on optimized incremental support vector machine," in *Pattern Recognition*, S. Li, C. Liu, and Y. Wang, Eds. Berlin, Heidelberg: Springer, 2014, pp. 595–603.

[27] H. Wu, X. Liu, Y. Xiao, and Y. Rao, "A dynamic time sequence recognition and knowledge mining method based on the hidden Markov models (HMMS) for pipeline safety monitoring with ϕ-OTDR," *J. Lightw. Technol.*, vol. 37, no. 19, pp. 4991–5000, Oct. 2019.

[28] I. Guyon and A. Elisseeff, *An Introduction to Feature Extraction*. Berlin, Heidelberg: Springer, 2006, pp. 1–25.

[29] M. Adeel, C. Shang, K. Zhu, and C. Lu, "Nuisance alarm reduction: Using a correlation based algorithm above differential signals in direct detected phase-OTDR systems," *Opt. Express*, vol. 27, no. 5, pp. 7685–7698, Mar. 2019.

[30] Z. Sha, H. Feng, and Z. Zeng, "Phase demodulation method in phase-sensitive OTDR without coherent detection," *Opt. Express*, vol. 25, no. 5, pp. 4831–4844, Mar. 2017.

[31] Z. Qin, H. Chen, and J. Chang, "Detection performance improvement of distributed vibration sensor based on curvelet denoising method," *Sensors*, vol. 17, no. 6, p. 1380, 2017.

[32] P. Zhu, C. Xu, W. Ye, and M. Bao, "Self-learning filtering method based on classification error in distributed fiber optic system," *IEEE Sensors J.*, vol. 19, no. 19, pp. 8929–8933, Oct. 2019.

[33] F. Jiang, H. Li, Z. Zhang, Y. Zhang, and X. Zhang, "Localization and discrimination of the perturbation signals in fiber distributed acoustic sensing systems using spatial average Kurtosis," *Sensors*, vol. 18, no. 9, 2018, Art. no 2839.

[34] J. Tejedor, J. Macias-Guarasa, H. F. Martins, J. Pastor-Graells, P. Corredera, and S. Martin-Lopez, "Machine learning methods for pipeline surveillance systems based on distributed acoustic sensing: A review," *Appl. Sci.*, vol. 7, no. 8, 2017.

[35] J. Tejedor *et al.*, "Real field deployment of a smart fiber-optic surveillance system for pipeline integrity threat detection: Architectural issues and blind field test results," *J. Lightw. Technol.*, vol. 36, no. 4, pp. 1052–1062, Feb. 2018.